https://doi.org/10.5194/egusphere-2024-2454
Preprint. Discussion started: 6 August 2024

Isomer Molecular Structures and Formation Pathways of Oxygenated Organic Molecules in Newly Formed Biogenic Particles

Vignesh Vasudevan-Geetha[1], Lee Tiszenkel[1], Zhizhao Wang[2,3], Robin Russo[4], Daniel J. Bryant[5], Julia Lee-Taylor[3], Kelley C. Barsanti[3], Shan-Hu Lee[1,4*]

[1]Department of Atmospheric and Earth Sciences, University of Alabama in Huntsville, Huntsville, AL 35805, United States

[2]Department of Chemical and Environmental Engineering, University of California - Riverside, Riverside, CA 92521, United States

[3]Atmospheric Chemistry Observation & Modeling Laboratory, National Center for Atmospheric Chemistry, Boulder, CO 30807, United States

[4]Department of Chemistry, University of Alabama in Huntsville, Huntsville, AL 35805, United States

[5]Department of Chemistry, University of York, York, YO10 5DD, United Kingdom

*Corresponding author (shanhu.lee@uah.edu)

Abstract

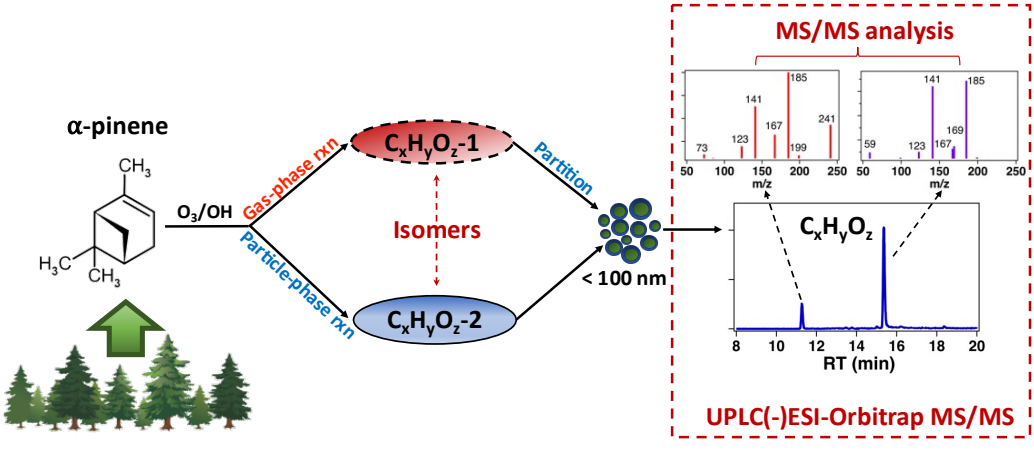

Oxygenated organic molecules (OOMs) formed from oxidation of anthropogenic and biogenic volatile organic compounds (VOCs) are essential ingredients for atmospheric new particle formation (NPF) and secondary organic aerosol (SOA) formation, and thus impact air quality, human health, and climate. There is a large variety of OOM compounds, but currently, for the vast majority of OOMs, their molecular structures and formation pathways are still unknown. In this

https://doi.org/10.5194/egusphere-2024-2454
Preprint. Discussion started: 6 August 2024

study, we identified isomer-resolved molecular structures and reaction pathways for dimer OOMs formed from α-pinene ozonolysis, using an ultrahigh-performance liquid chromatography-electrospray ionization Orbitrap mass spectrometer (UPLC/(-)ESI-Orbitrap MS) tandem analysis and a high-resolution time-of-flight chemical ionization mass spectrometer (HrTOF-CIMS) attached to the filter inlet for gas and aerosol (FIGAERO), combined with explicit chemical modeling simulations using the Generator of Explicit Chemistry and Kinetics of Organics in the Atmosphere (GECKO-A). In general, each OOM identified in the newly formed biogenic particles contains 2-8 isomers with distinctive MS/MS fragmentation ions. For $C_{19}H_{30}O_5$, which is one of most abundant dimers identified from the boreal forests and laboratory biogenic NPF studies, one isomer forms in the gas phase from a stabilized Crigee Intermediate (sCI) peroxy biradical and aldehyde, followed by subsequent gas-to-particle conversion; and another isomer forms in the particle phase via the Baeyer-Villiger reaction from a cyclic acylperoxyhemiacetal and α-pinanediol. Two isomers of $C_{16}H_{26}O_6$ form in the particle phase via decarboxylation from two different isomers of $C_{17}H_{26}O_8$ after the condensation from the gas phase. Thus, our results show that biogenic OOMs can also form from particle-phase reactions and have different isomeric structures than in the gas phase. Our study represents the first molecular-level chemical analysis to identify particle-formation pathways for OOMs in the newly formed biogenic nanoparticles. Currently, parameterizations of NPF (e.g., biogenic NPF) are based on the gas-to-particle conversion of extremely low-volatility OOM dimers that form in the gas phase alone (e.g., via RO_2 + RO_2 reactions). Our study demonstrates that additional, independent particle-phase formation pathways should also be considered for predictions of the formation and growth of new particles in the atmosphere.

Keywords. OOMs, particle-phase reaction, gas-to-particle conversion, new particle formation, isomer, MS/MS tandem analysis

Synopsis: This study highlights the importance of particle-phase reactions that are currently not considered in the new particle formation processes.

https://doi.org/10.5194/egusphere-2024-2454
Preprint. Discussion started: 6 August 2024

1. Introduction

Oxygenated organic molecules (OOMs) formed from oxidation reactions of biogenic volatile organic compounds (BVOCs) can contribute to secondary organic aerosol (SOA) and new particle formation (NPF) processes [*Barsanti et al.*, 2017; *Bianchi et al.*, 2019; *Hallquist et al.*, 2009; *S-H Lee et al.*, 2019; *Ziemann and Atkinson*, 2012]. In the atmosphere, BVOCs are oxidized by ozone, hydroxy (OH), and nitrate (NO_3) radicals. There are many OOMs in the atmosphere with different chemical identities (e.g., chemical formulas and isomeric structures). For example, from ozonolysis of α-pinene alone, thousands of OOMs were detected with different mass-to-charge ratios (m/z) with a high-resolution time-of-flight chemical ionization mass spectrometer (HrTOF-CIMS), hence, indicating different chemical formulas (e.g., [*Caudillo et al.*, 2021; *Lee Tiszenkel and Lee*, 2023]). Yet, only an extremely limited number of OOMs have been identified with their isomer molecular structures and formation pathways, even for the α-pinene ozonolysis system, which is the most-studied biogenic oxidation system in the atmospheric chemistry field. Previous studies have made isomer structural analysis of biogenic OOMs mostly for SOA particles and still, detailed molecular structures of OOMs in newly formed pure biogenic particles are not known.

In the gas phase, dimeric OOMs form from reactions involving organic peroxy radicals (RO_2) [*Peräkylä et al.*, 2023; *Tomaz et al.*, 2021; *Wang et al.*, 2023] and stabilized Criegee intermediates (sCI) [*Y Zhao et al.*, 2015; *Y Zhao et al.*, 2022]. Particle-phase formation of dimeric OOMs involves esterification [*Müller et al.*, 2008; *Yasmeen et al.*, 2010], Baeyer-Villiger reactions [*Claflin et al.*, 2018; *Kenseth et al.*, 2023; *Pospisilova et al.*, 2020], aldol condensation [*Tolocka et al.*, 2004; *Witkowski and Gierczak*, 2014; *Ziemann and Atkinson*, 2012], diacyl decomposition [*Zhang et al.*, 2015], and acyl trioxide decomposition [*Kahnt et al.*, 2018]. Isomer-resolved characterization of these OOMs was made possible using liquid chromatographic techniques; and high-resolution mass spectrometer coupled with tandem MS/MS analysis enabled the elucidation of molecular structures of BVOC oxidation products [*Nozière et al.*, 2015]. For α-pinene oxidation SOA, the dimer esters, $C_{17}H_{26}O_8$ (*m/z* = 358) and $C_{19}H_{28}O_7$ (*m/z* = 368), have been structurally resolved using a linear ion trap mass spectrometer and it was shown that they form from acyl trioxide decomposition of a gas-phase product dimer $C_{19}H_{28}O_{11}$ by *Kahnt et al.* [2018]. *Zhang et al.* [2015] proposed the structure of the dimers in the particle phase using electrospray ionization-quadrupole time of flight mass spectrometer (ESI-QTOF-MS), of which $C_{17}H_{26}O_6$ (m/z = 309) forms from decarboxylation reaction. *Kristensen et al.* [2016] identified the structure of specific dimer esters from α-pinene ozonolysis experiments, which were also identified from the boreal forest ambient samples identified using ESI-QTOF-MS. *Kenseth et al.* [2023] illustrated the particle-phase accretion reaction and subsequent formation of $C_{19}H_{30}O_5$ (*m/z* = 337) through Baeyer-Villiger decomposition reaction. In addition to the α-pinene oxidation SOA, MS/MS analysis has also been used to study other monoterpene oxidation products such as limonene-derived products using online-nitrate chemical ionization Orbitrap MS/MS by *Tomaz et al.* [2021], β-pinene-derived products using liquid chromatography (LC) coupled with ESI-QTOF-MS [*Kenseth et al.*, 2018] and molecular analysis of SOA derived from monoterpenes such as α-pinene, β-pinene, limonene, 3-carene and sabinene using LC coupled with ion trap mass spectrometer by *Glasius et al.* [2000].

https://doi.org/10.5194/egusphere-2024-2454
Preprint. Discussion started: 6 August 2024

The current understanding of the NPF processes is based on the gas-to-particle conversion of low-volatility chemical precursors [*S-H Lee et al.*, 2019]. It is assumed that OOMs form in the gas phase, and the OOMs that have sufficiently low volatilities undergo gas-to-particle conversion to contribute to the formation and growth of new particles. Therefore, particle phase formation of OOMs is not considered in the current NPF theories and parameterizations. Typically, the volatility (or saturation vapor concentration at a specific temperature) of an OOM moiety is estimated with the Volatility Basis Set (VBS) parameterization [*Donahue et al.*, 2011], where the elemental composition of C, O, and N dictates saturation vapor concentration [*Ye et al.*, 2019]. Volatilities can be also derived from thermogram measurements using a filter inlet for gas and aerosols (FIGAERO) attached to a high-resolution time-of-flight chemical ionization mass spectrometer (HrTOF-CIMS) [*Lopez-Hilfiker et al.*, 2014]. Laboratory experiments have shown that the volatilities derived from these two methods have systematic discrepancies for OOMs formed from ozonolysis of α-pinene (e.g., VBS over-estimates volatilities for monomers and under-estimates for dimers compared to FIGAERO) [*Lee Tiszenkel and Lee*, 2023].

In this work, we have analyzed the molecular composition of OOMs formed from the ozonolysis of α-pinene using an ultra-performance liquid chromatography-electrospray ionization Orbitrap mass spectrometry (UPLC/(-)ESI-Orbitrap MS) and HrTOF-CIMS coupled with a FIGAERO. The chemical composition of OOMs in the gas and aerosol phase was measured simultaneously with FIGAERO HrTOF-CIMS. The liquid chromatogram separates isomers of OOMs, and the most likely molecular structures of an isomer were derived based on the fragmentation ions detected with high-resolution Orbitrap MS/MS analysis. To help verify the molecular structures of OOMs in the gas phase, we also performed simulations with the chemically explicit model, the Generator of Explicit Chemistry and Kinetics of Organics in the Atmosphere (GECKO-A) ([*Aumont et al.*, 2005; *Camredon et al.*, 2007; *Valorso et al.*, 2011]; updated per [*Jenkin et al.*, 2020; *Jenkin et al.*, 2019; *Jenkin et al.*, 2018]). Based on these analyses, we propose the isomeric structures of two dimer OOMs ($C_{19}H_{30}O_5$ and $C_{16}H_{26}O_6$) and their potential formation pathways in the gas and aerosol phase.

2. Materials and Methods

Experiments were carried out in the Tandem Aerosol Nucleation and Growth Environment Tube (TANGENT) setup. A detailed description of this experimental setup has been published previously [*Lee Tiszenkel and Lee*, 2023; *L. Tiszenkel et al.*, 2019]. Briefly, 240 ppb α-pinene in nitrogen was mixed with 1200 ppb O_3 at room temperature (298 K) and dry conditions (RH < 10%). The total residence time in the flow tube was 150 s. The OH radicals present in the experimental system were the byproduct of the monoterpene ozonolysis reaction. Experiments were done without an OH scavenger and without seed aerosols. A chemical box model using the Master Chemical Mechanism (MCM v3.3.1) [*Jenkin et al.*, 2015] was used to estimate the OH radical concentration in the experimental setup at 1.6 ppt. Aerosol size distributions from 1-80 nm were measured by combining data from a particle size magnifier (PSM; A10, Airmodus) and a scanning mobility particle sizer (SMPS; Model 3080 electrostatic classifier, model 3776 condensation particle counter CPC, and model 3085 differential mobility analyzer DMA, TSI Inc.).

2.1. Filter Inlet for Gases and Aerosols on High Resolution Time of Flight Chemical Ionization Mass Spectrometer (FIGAERO Hr-TOF CIMS)

https://doi.org/10.5194/egusphere-2024-2454
Preprint. Discussion started: 6 August 2024

The chemical composition of OOMs in the gas and aerosol phase was measured online by an iodide HrTOF-CIMS attached to FIGAERO [*B H Lee et al.*, 2014] (Aerodyne Inc.). The HrTOF has a mass resolution (m/Δm) of 7,000. During gas-phase sampling, the FIGAERO drew 2 LPM from the flow tube through a 0.64 cm OD stainless steel line onto a Teflon filter (Zerflour® 24 mm diameter, 2 µm pore size, Pall Corp) for 20 minutes of particle collection. The FIGAERO then directed the filter into a flow of dry ultra-high purity (UHP) nitrogen for thermal desorption of the collected particles. The nitrogen was heated from room temperature at a rate of 35 ºC per minute for 5 minutes to a final temperature of 200 ºC. The filter was then heat soaked with a flow of 200 ºC nitrogen for an additional 15 minutes. The maximum vaporization temperature (T_{max}) during thermal desorption was used to derive the saturation vapor concentration (C*) of the OOMs based on calibration of the FIGAERO with polyethylene glycols with known C* [*Lee Tiszenkel and Lee*, 2023]. The FIGAERO T_{max} is subject to variability depending on the filter mass loading and thermally driven particle-phase chemistry [*Huang et al.*, 2020]. Gas-phase concentrations of species measured with the HrTOF-CIMS were calculated by assuming that OOM sensitivity was equivalent to the formic acid sensitivity. This assumption is reasonable to within a factor of 1.5 [*Lopez-Hilfiker et al.*, 2015]. Calibration of the HrTOF-CIMS using a formic acid permeation source (Kin-Tek) yielded a sensitivity of 6.7 Hz ppt^{-1} MHz^{-1}. The detection limit (defined as the signal with a S/N ratio of 3) was 4.3 pptv. Uncertainties in this calibration factor, taking into account errors in flow meters, permeation sources, and calibration, were calculated as 16%.

2.2. Filter sample collection and extraction

Particles were collected on Whatman® glass microfiber filters (Grade GF/D, 2.7 µm pore size, 25mm diameter), which were pre-baked at 550 ºC for 24 hours to remove any residual organics. The particles were collected continuously for 28 hours with a 1 L/min flow through the filter from the experimental tube to generate approximately 500 µg of aerosol samples. Filters were moved to borosilicate glass vials for storage at -20 ºC immediately after collection to prevent any significant changes to the OOM chemical composition and their abundance [*Resch et al.*, 2023]. Three replicate filters were collected from similar experimental conditions.

Filter samples were divided into quarters and each quarter was separately extracted by sonicating for 30 minutes in borosilicate glass vials with 20 mL methanol (Optima™ LC/MS, Fisher Scientific) placed in beakers filled with ice. After 30 minutes, the ice was replaced and the sample was sonicated for additional 30 minutes. The sample was then dried down under a weak stream of pure nitrogen gas in a room-temperature water bath. The dried sample was reconstituted in 2 mL of methanol and filtered through a 0.2 um nylon syringe filter (ThermoFisher Scientific) into a sampling vial for LC analysis. Previous studies have shown that organic peroxides decay relatively slowly in 100% methanol [*R Zhao et al.*, 2018a; *Y Zhao et al.*, 2015; *Y Zhao et al.*, 2022]. Procedural blanks were prepared by subjecting filters that had undergone the pre-baking process to the same extraction procedures.

2.3. Ultrahigh-Performance Liquid Chromatography/Negative Electrospray Ionization Orbitrap Mass-Spectrometry (UPLC/(-)ESI-Orbitrap MS)

The filter samples were chromatographically separated and analyzed using ultrahigh-performance liquid chromatography (UPLC) (Vanquish, ThermoFisher Scientific) coupled to an ultra-high resolution Orbitrap mass spectrometer (Exploris 120 MS, ThermoFisher Scientific) with an

https://doi.org/10.5194/egusphere-2024-2454
Preprint. Discussion started: 6 August 2024

electrospray ionization (ESI) source. The orbitrap has a mass resolution (m/Δm) of 120,000 for MS and 15,000 for MS/MS analysis. The separation of compounds including isomers was achieved using a 100 mm x 2.1 mm reverse phase C-18 column with 1.8 um particle size (Waters, ACQUITY Premier HSS T3). The column and autosampler temperatures were maintained at 40 ºC and 4 ºC , respectively. The polar (A) and non-polar (B) mobile phase solvents were 0.1% formic acid in ultra-pure water (Optima™ LC/MS, Fisher Scientific) and 0.1% formic acid in MeOH (Optima™ LC/MS, Fisher Scientific) respectively. Gradient elution was performed starting with 1-minute post-injection hold at 90% A and 10% B followed by a decrease to 10% A and 90% B over 26 minutes, then a return to 90% A and 10% B over 2 minutes, and ending with a 2 minute column equilibration, as adopted from [*Shao et al.*, 2022]. The total flow rate was 0.3 mL min^{-1} with an injection volume of 2 µL; these conditions were determined by optimizing the *cis*-pinic acid (*m/z* 185) signal for maximum peak area. The non-targeted mass spectrometric analysis was carried out using optimized ESI parameters: 2.5 kV capillary voltage; 325 ºC ion transfer tube temperature; 350 ºC vaporizer temperature, and 50, 10, and 1 (arbitrary units) flow rates for sheath gas, auxiliary gas and sweep gas, respectively. The parent molecules were deprotonated using (-)ESI and were detected as $[M-H]^-$ ions, also protonated by (+)ESI, and were detected as $[M+H]^+$ and $[M+Na]^+$ ions. This study is mostly based on the negative ionization results. Unscheduled (RT not specified) and non-targeted tandem mass spectrometric (MS/MS) analyses were performed using higher-energy collisional dissociation (HCD) with a stepped normalized collision energy of 20%, 40%, and 60% for those compounds detected with an ion intensity threshold of 5×10^3. Post-acquisition data processing was carried out using a non-targeted compound identification method developed in Compound Discoverer software (version 3.3 SP2, ThermoFisher Scientific). Additional details are given in Supplementary Information.

Combining these two independent high-resolution mass spectrometer techniques, HrTOF-CIMS and UPLC/(-)ESI-Orbitrap MS, provides a very powerful tool for analyzing the particle-phase chemical composition of OOMs, for identifying molecular structures of different isomers. So far, only a few studies have combined these two methods to make molecular-level chemical speciation of OOMs (e.g., [*Du et al.*, 2022; *Huang et al.*, 2020; *Mehra et al.*, 2020]). It is noted that HrTOF-CIMS (iodide ionization) and UPLC/(-)ESI-Orbitrap MS may have different ionization efficiencies and detection efficiencies for different chemical compounds. Additionally, offline filter sample analysis can introduce some artifacts during sampling collection, storage, and extraction processes.

2.4. GECKO-A simulations

To help verify the chemical reactants and products of a-pinene ozonolysis reactions in the gas phase, as well as their molecular structures, we generated an explicit α-pinene degradation mechanism using GECKO-A ([*Aumont et al.*, 2005; *Camredon et al.*, 2007; *Valorso et al.*, 2011]; updated per [*Jenkin et al.*, 2020; *Jenkin et al.*, 2019; *Jenkin et al.*, 2018]), and performed model simulations using the box model. GECKO-A is a state-of-the-art automatic mechanism generator designed to produce explicit oxidation degradation schemes for organic compounds. Detailed mechanism description and simulation procedures used in this study are described in the Supporting Information.

3. Results and discussions

https://doi.org/10.5194/egusphere-2024-2454
Preprint. Discussion started: 6 August 2024

3.1. Overall molecular composition of oxygenated organic molecules in α-pinene ozonolysis system

Figure S1 shows the measured aerosol size distribution with a mean diameter of 70 nm during the typical experiment. We chose only the 50% most abundant OOMs in the present study. Figure 1 shows the total ion mass spectra and the mass defect plots the OOMs detected using LC-Orbitrap MS, FIGAERO-CIMS, and HrTOF-CIMS. In all mass spectra, clearly, monomers (C_5-C_{10}) and dimers (C_{15}-C_{20}) were resolved. In the gas phase, there were relatively high ion intensities for monomers than dimers, whereas relative ion intensities of dimers increased in the particle phase (as shown in both FIGAERO-CIMS and UPLC/(-)ESI-Orbitrap MS), indicating that dimers, in general, are more favorable for gas-to-particle conversion due to relatively lower volatilities, consistent with previous observations [*Lee Tiszenkel and Lee*, 2023]. Notably, the particle-phase OOM spectra taken by UPLC/(-)ESI-Orbitrap MS and FIGAERO-CIMS show strikingly similar patterns, despite the entirely different sampling (offline versus online) and ionization methods and potential artifacts introduced during the filter collection, storage, and extraction procedures. There were also many more small ions ($C_{5\text{-}6}$) detected with the FIGAERO-CIMS than in the LC-Orbitrap mass spectrometer, likely due to the thermal fragmentation of OOMs during the desorption cycle in the FIGAERO. As shown in Figure 1g, many OOMs detected by LC-Orbitrap MS showed 2-8 isomers (discussed in detail in Section 3.3), but these isomers were not resolved in FIGAERO-CIMS.

In total, 167 OOMs were identified with UPLC/(-)ESI-Orbitrap MS, 405 OOMs were identified in the particle phase with the FIGAERO -CIMS, and 437 OOMs were identified in the gas phase with the HrTOF-CIMS (Figure 1h). Of the 588 OOMs detected, 304 OOMs were found in both the gas and particle phases, suggesting that these are OOMs that likely underwent gas-to-particle conversion. However, there were 124 OOMs that were detected in the gas phase alone, and 151 OOMs that were detected only in the particle phase (by the FIGAERO-CIMS and UPLC/(-)ESI-Orbitrap MS). Further discussions of particle-phase OOMs will concern 77 compounds selected from the 108 detected in the particle-phase by the FIGAERO-CIMS and UPLC/(-)ESI-Orbitrap MS. Table S1 shows the chemical formula of OOMs detected in HrTOF-CIMS (gas and particle phases) and UPLC/(-)ESI-Orbitrap MS (particle phase). Table S2 lists these OOM compounds, along with their isomers defined by their distinct RT and tandem MS/MS fragmentation ions of each isomer. These compounds were selected by considering the reproducibility of their desorption thermograms.

3.2. FIGAERO measured versus VBS calculated saturation vapor concentration

Figure 2 shows the saturation vapor concentrations (C*) of the OOMs derived from FIGAERO thermogram measurements and VBS parameterization. FIGAERO measured saturation vapor concentrations (C*) classify the OOMs in the range between extremely-low-volatility organic compounds (ELVOC) and semi-volatile organic compounds (SVOC). For the same set of OOMs, VBS-derived saturation vapor concentrations have a wider range, from ultra-low-volatility organic compounds (ULVOC) to intermediate-volatility organic compounds (IVOC). Regardless, there was the same trend of decreasing saturation vapor concentration with increasing molecular weight for both methods (Figures 2c and S2). Some OOMs (e.g., $C_{10}H_{14}O_6$, $C_{10}H_{16}O_6$, $C_{11}H_{16}O_6$, $C_{12}H_{20}O_5$, $C_{14}H_{20}O_8$, $C_{15}H_{22}O_6$, $C_{15}H_{24}O_8$, $C_{15}H_{26}O_6$, $C_{17}H_{26}O_8$, $C_{17}H_{28}O_5$ and $C_{18}H_{30}O_7$) showed

https://doi.org/10.5194/egusphere-2024-2454
Preprint. Discussion started: 6 August 2024

a better agreement between FIGAERO measurements and VBS calculations. Remarkably, both methods were able to replicate the "teeth-like" feature observed in measured saturation vapor concentration with increasing molecular weight, oxygen, and carbon numbers, as predicted from the VBS parameterizations.

However, there were general discrepancies in saturation vapor concentration from these two methods. While volatilities derived with these two methods were more correlated to each in the middle-number carbons (e.g., $C_{10\text{-}15}$), they deviated by several orders of magnitude at the smaller and larger carbon numbers, consistent with our previous study [*Lee Tiszenkel and Lee*, 2023]. For example, the VBS-calculated volatilities overestimate FIGAERO measurements by 4 orders of magnitude for C5 and underestimate FIGAERO measurements by 4 orders of magnitude for C20 OOMs. FIGAERO measurements also show that the $C_{16\text{-}17}$ compounds have the lowest measured volatility, in contrast to the VBS calculations that estimate C_{20} OOMs are the least volatile. We also find that the trend in measured volatilities for some series of OOMs deviated from the trend expected with VBS estimation. For example, VBS estimated the decreasing volatility with increasing oxygen number for $C_{10}H_{14}O_{4\text{-}6}$, while FIGAERO measurements showed an increase in volatility from 4 to 6 oxygen atoms. Another discrepancy arises when comparing the FIGAERO and VBS for compounds with a constant number of carbon or oxygen but differing hydrogen numbers such as $C_8H_{12\text{-}14}O_6$ or $C_9H_{14\text{-}16}O_6$. Here, the saturation vapor pressure tended to be higher by 1-3 orders of magnitude for the compounds containing fewer hydrogen. The opposite was true with dimers such as $C_{19}H_{28\text{-}30}O_7$ and $C_{19}H_{28\text{-}30}O_6$. These observations are consistent with [*Hyttinen et al.*, 2021; *Kurtén et al.*, 2016] that in the case of monomers, an increase in intermolecular hydrogen bonding by hydrogen-donor functional groups likely decreases the volatility, while dimers with more hydrogen atoms can favorably form intramolecular hydrogen bonds, which make them more stable in the gas-phase. Hydrogen bonding, functional groups, and structural differences between isomeric compounds affect volatilities [*Pankow and Asher*, 2008; *West et al.*, 2023], but these processes are not considered in the current VBS parameterizations. For some OOMs (e.g., $C_8H_{14}O_5$ and $C_{20}H_{32}O_6$), we observed multimodal peaks in the FIGAERO thermogram (Figure S3), which is likely due to the presence of isomeric compounds. Thus, isomeric compounds can affect the shape (and peak location) of the desorption peak (T_{max}) for a certain OOM moiety and hence, influence the estimation of the saturation vapor concentration.

3.3. Molecular structures and reaction pathways of dimer OOM isomers

Isomers were identified in the liquid chromatogram, as they have different interactions with the column material due to their unique chemical structures and so can be effectively separated at different retention times (RT). The UPLC/(-)ESI-Orbitrap mass spectrometer detected 77 OOM compounds different m/z values. When including their isomers, which had distinctive MS/MS fragmentation ions and hence different molecular structures, there were in total 277 compounds (Figure 1g).

$C_{19}H_{30}O_5$ (m/z = 337) is one of the major dimers produced from α-pinene ozonolysis, as has been previously detected in boreal forests [*Kristensen et al.*, 2016] and laboratory studies [*Kenseth et al.*, 2023; *Y Zhao et al.*, 2018b]. Figure 3a shows the EIC of $C_{19}H_{30}O_5$, indicating six isomers that eluted at different retention times. Figures 3b and 3c show MS/MS spectra of two main isomers $C_{19}H_{30}O_5$-1 (RT = 15.3 min) and $C_{19}H_{30}O_5$-2 (RT = 20.2 min). The distinctive MS/MS

https://doi.org/10.5194/egusphere-2024-2454
Preprint. Discussion started: 6 August 2024

fragmentation ions from these two compounds indicate that these two isomeric compounds have structural differences. Based on its MS/MS fragmentation ions, we have derived its chemical structure containing secondary ozonide (SOZ) for $C_{19}H_{30}O_5$-1 (Scheme S1). Due to the unique SOZ structure, there are three main fragmentations, leading to 3 pairs of daughter ions (m/z = 213/123, 167/169, and 183/153). These daughter ions further fragment by losing H_2O, CO, or C_2H_3O to form smaller ions (m/z 195, 125, and 141). The parent SOZ also loses H_2O to form another daughter ion (m/z = 319). All these fragmentation ions appeared in the MS/MS spectrum (Figure 3b). There were additional two fragmentation ions (m/z = 293 and 275) which we cannot identify their structures. Based on the SOZ structure, we propose that the $C_{19}H_{30}O_5$-1 isomer forms from the gas phase dimerization of a stabilized Criegee intermediate (sCI) and norpinonaldehyde ($C_9H_{14}O_2$), and further undergoes gas-to-particle conversion (Figure 3d). These reactants, including their specific molecular structures, were reproduced by the GECKO-A modeling simulations from a-pinene ozonolysis (Table S3). Previously, *Y Zhao et al.* [2022] also proposed a SOZ molecular structure for $C_{20}H_{32}O_5$ from α-pinene ozonolysis, and indicated the same dimer formation pathway from bimolecular reactions involving sCI. On the other hand, our proposed reaction mechanism contrasts with the particle-phase aldol condensation route for $C_{19}H_{30}O_5$ proposed by *Witkowski and Gierczak* [2014], although they showed similar fragmentation patterns (as shown in Scheme S1).

The MS/MS spectrum for $C_{19}H_{30}O_5$-2 (RT = 20.2 min) (Figure 3c) shows the same fragmentation ions as shown previously by [*Kenseth et al.*, 2023; *Kristensen et al.*, 2016]. As illustrated in Scheme S2, there are two main fragmentations near the ester function group, leading to 2 pairs of daughter ions (m/z= 169/167 and 151/185). The m/z = 185 undergoes subsequent fragmentations by losing CO_2, H_2O, then C_3H_6 to form m/z = 141, 123, then 81, respectively. Previously, [*Kenseth et al.*, 2023] showed that this isomer forms in the particle phase from cyclic acylperoxyhemiacetal (m/z = 185) and α-pinanediol (m/z 193), via nucleophilic addition followed by Baeyer-Villiger decomposition reaction (Figure 3e). Cyclic acylperoxyhemiacetal is the isomerization product of *cis*-3-peroxy pinalic acid. The GECKO-A model predicted the formation of *cis*-3-peroxy pinalic acid and α-pinanediol in the gas phase (Table S3), with the same molecular structures as shown in Figure 3e. These two compounds were also identified in the particle phase with UPLC/(-)ESI-Orbitrap mass spectrometer (e.g., Figure S4). Thus, our analysis demonstrates that the accretion reaction of $C_{19}H_{30}O_5$-2, which takes place within SOA particles [*Kenseth et al.*, 2023], also occurs in newly formed biogenic particles.

Thus, while $C_{19}H_{30}O_5$-1 forms in the gas phase via bimolecular reactions involving sCI followed by gas-to-particle conversion, $C_{19}H_{30}O_5$-2 forms within the particle phase via esterification. These proposed mechanisms are qualitatively consistent with *Y Zhao et al.* [2022] that one of $C_{19}H_{30}O_5$ isomers was reduced when a sCI scavenger was introduced into the system (very likely $C_{19}H_{30}O_5$-1), while another isomer of $C_{19}H_{30}O_5$ did not change in abundance when sCI scavenger was used (possibly $C_{19}H_{30}O_5$-2).

To further understand the relative contribution of these two processes discussed above, gas-to-particle conversion of $C_{19}H_{30}O_5$-1 versus particle-phase Baeyer-Villiger reaction for $C_{19}H_{30}O_5$-2, we changed relative concentrations of oxidants (Figure S5). We observed a lower abundance of $C_{19}H_{30}O_5$-2 compared to $C_{19}H_{30}O_5$-1 when the oxidation system was dominated by ozone rather

https://doi.org/10.5194/egusphere-2024-2454
Preprint. Discussion started: 6 August 2024

than OH (ozone = 1200 ppb, OH = 1.6 ppt, $k_{\alpha\text{-pinene* O3}}$ = 9 x 10^{-17} cm^3 $molecule^{-1}$ s^{-1} and $k_{\alpha\text{-pinene* OH}}$ = 5.3 x 10^{-11} cm^3 $molecule^{-1}$ s^{-1} [*Atkinson et al.*, 2006]). However, when ozone concentration was varied from 250-1000 ppb, $C_{19}H_{30}O_5$-1 abundance was reduced compared to experiments at higher ozone, but $C_{19}H_{30}O_5$-2 abundance remained constant. This is because $C_{19}H_{30}O_5$-1 formation was dependent on gas-phase precursor concentration, while $C_{19}H_{30}O_5$-2 formed from particle-phase reactions. Clearly, isomeric compounds can be formed independently from both gas- and particle-phase reaction pathways to contribute to the particle mass, and which isomer becomes dominant depends on the atmospheric conditions.

There were 12 compounds detected only in the particle phase, without their gas-phase counterparts (Figure 1h and Table S1), implying that these compounds form via particle-phase reactions (as opposed to gas-to-particle conversion). Among these compounds, $C_{16}H_{26}O_6$ (*m/z* = 313) has been identified in the particle phase in previous studies [*Huang et al.*, 2020; *Kristensen et al.*, 2016; *Zhang et al.*, 2015]. Here we propose that two isomers of $C_{16}H_{26}O_6$ form exclusively in the particle phase via decarboxylation from two isomers of $C_{17}H_{26}O_8$ (as opposed to gas-to-particle conversion).

The EIC of $C_{16}H_{26}O_6$ shows the presence of five isomers eluting out at different RTs (Figure 4a). The fragmentation spectra of the two most abundant isomers, $C_{16}H_{26}O_6$-1 (RT = 16.6 min) and $C_{16}H_{26}O_6$-2 (RT = 18.4 min), are shown in Figures 4b and c, respectively. The proposed structure and fragmentation mechanism of $C_{16}H_{26}O_6$-1 is presented in Scheme S3. The fragmentation ions of $C_{16}H_{26}O_6$-1 agree with those shown by [*Kristensen et al.*, 2016], although this cited study did not show the molecular structure of this compound. Fragmentation of the parent ion of $C_{16}H_{26}O_6$-1 yields one daughter ion (m/z = 185), which fragments into three smaller ions: m/z = 167 by losing water, and two isomers with m/z = 141 by losing CO_2. The two isomers further fragment into smaller ions with m/z = 123 and 71 by losing H_2O and C_5H_{10}, respectively. Another small ion with *m/z* = 57 is fragmented from the parent molecule. These fragmentation ions are consistent with those shown in the MS/MS spectrum (Figure 4b). Figure 4d illustrates the reaction pathway for the $C_{16}H_{26}O_6$-1 isomer proposed in this study. First, the precursor molecule ($C_{17}H_{26}O_8$) forms by the RO_2 + RO_2 gas-phase dimerization of $C_9H_{14}O_5$ and $C_8H_{14}O_5$. Upon partitioning to the particle phase, $C_{17}H_{26}O_8$ undergoes the decarboxylation reaction to form $C_{16}H_{26}O_6$-1. The HrTOF-CIMS measured both the reactants ($C_9H_{14}O_5$ and $C_8H_{14}O_5$) in the gas phase, while $C_{17}H_{26}O_8$ was detected both in the gas and particle phase (Table S1). The GECKO-A model also simulated the reactants with the same molecular structures (Table S3) as shown in Figure 4d.

For the second isomer, $C_{16}H_{26}O_6$-2, fragmentation of the parent molecule at the ester linkage results in daughter ions with *m/z* = 171 and 141 (Scheme 4). Loss of CO_2 from *m/z* 171 produces a fragmentation ion *m/z* = 123, which subsequently loses H_2O to form *m/z* = 109. These fragmentation ions are consistent with the MS/MS spectrum shown in Figure 4c. We propose that $C_{17}H_{26}O_8$ -2 forms in the gas phase by the $RO_2^{\cdot}$ + $RO_2^{\cdot}$ dimerization from $C_9H_{14}O_4^{\cdot}$ and $C_8H_{14}O_6^{\cdot}$ (both were detected in the gas phase), followed by gas-to-particle conversion, and further undergoes particle-phase decarboxylation to form the dimer $C_{16}H_{26}O_6$-2 in the particle phase (Figure 4e). Thus, the two isomers of $C_{16}H_{26}O_6$ form from the particle-phase decomposition reactions of two isomers of $C_{17}H_{26}O_8$, while $C_{16}H_{26}O_6$ was not detected in the gas phase.

https://doi.org/10.5194/egusphere-2024-2454
Preprint. Discussion started: 6 August 2024

The cumulative signal fractions of OOMs showed higher ion intensities of $C_{15\text{-}19}$ species than C_{20} in the UPLC/(-)ESI-Orbitrap MS (Figure S7). Interestingly, there were also more different compounds (and their isomers) within $C_{15\text{-}19}$ than C_{20}. The increased $C_{15\text{-}19}$ dimer abundance compared to C_{20} dimers was also seen in previous chamber studies, where the particle-phase chemical evolution of dimers measured in real-time using extractive electrospray ionization-time of flight (EESI-TOF) mass spectrometer showed a slowly increasing abundance of $C_{16\text{-}18}$ dimers with decreasing C_{20} dimers [*Pospisilova et al.*, 2020]. The particle-phase decomposition reactions can explain these observations.

Atmospheric Implications

We have investigated the chemical composition of gas- and particles-phase OOMs generated from ozonolysis of α-pinene, including their isomeric molecular structures and potential reaction schemes, using two high-resolution mass spectrometers: HrTOF-CIMS equipped with the FIGAERO inlet and UPLC/(-)ESI-Orbitrap MS. The key result of this study is particle-phase formation of OOMs. For example, whereas one isomer $C_{19}H_{30}O_5$ (a key dimer formed from ozonolysis of α-pinene) is from gas-to-particle formation upon the formation in the gas phase via sCI and aldehyde dimerization, another isomer of $C_{19}H_{30}O_5$ forms in the particle phase via accretion reaction of α-pinanediol and cyclic acylperoxyhemiacetal. Likewise, two isomers of $C_{16}H_{26}O_6$ form from decarboxylation reactions exclusively in the particle phase. Our results highlight the dynamic reaction medium of the particle phase, where OOMs readily undergo particle-phase reactions such as accretion and decomposition to form OOMs with entirely different molecular structures. Thus, biogenic new particle formation or growth cannot be predicted solely based on the volatility of OOMs formed in the gas phase. Our study demonstrates that particle-phase formation and transformations of OOMs should also be considered in the biogenic NPF processes, as well as urban NPF (in the presence of monoterpenes).

Most OOMs produced from the ozonolysis of α-pinene have 2-8 isomers. These isomeric compounds have not been considered in the NPF mechanisms. Rather, typically, an extremely broader grouping of biogenic OOMs has been used, such as C_5, C_{10}, C_{15}, or C_{20} groups to understand biogenic NPF chemical mechanisms [*Heinritzi et al.*, 2020; *McFiggans et al.*, 2019; *Lee Tiszenkel and Lee*, 2023], regardless the different OOMs chemical identities and molecular structures. Our results show that the VBS parameterization devised for determining the volatility of organic compounds exhibits inconsistencies with the FIGAERO-measured saturation vapor concentrations for some OOMs, depending on monomer vs. dimer, or whether OOMs containing intermolecular vs. intramolecular hydrogen bonding. These two methods, VBS and FIGAERO thermogram, do not consider isomers of OOMs in the volatility estimation.

The analysis of OOM formation pathways presented here highlights the effectiveness of combined online HrTOF-CIMS and offline UPLC/(-)ESI-Orbitrap MS/MS analysis. HrTOF-CIMS is essential for understanding the chemical evolution of an organic compound in real time. The liquid chromatogram and high-resolution MS/MS analyses are necessary for identifying the molecular structures of isomers. Our study using these two independent high-resolution mass spectrometers demonstrates that, despite the various possible artifacts associated with sampling storage and extraction procedures used in the off-line method, the mass spectra of OOMs in the particle show strikingly similar features from these two methods. Thus, our results provide reestablished

https://doi.org/10.5194/egusphere-2024-2454
Preprint. Discussion started: 6 August 2024

confidence in using the UPLC/(-)ESI-Orbitrap MS/MS analysis for chemical composition and molecular structural analysis.

This study investigates the OOMs chemical composition in biogenic new particles. However, it is probable that similar particle-phase reactions also take place in SOA particles. Accounting for structurally resolved OOMs formed in gas- or particle-phase reaction mechanisms may help close the long-standing gap between model predictions and ambient measurements of SOA [*Hallquist et al.*, 2009].

Acknowledgements

This study was supported by funding from the National Science Foundation (NSF) (2209722, 2117389, and 2107916). The GECKO-A work is supported by the NSF National Center for Atmospheric Research, which is a major facility sponsored by the U.S. NSF under Cooperative Agreement No. 1852977.

Author Contributions

SHL designed the concept; VVG, LT, RR, and DJB performed experiments; VVG, LT, and SHL made data analysis; ZW, JTL, and KCB made modeling simulations; VVG, LT, and SHL wrote the manuscript; all co-authors commented on the manuscript.

Data and Code Availability

Data used in this study will be available upon request (shanhu.lee@uah.edu). The MS/MS spectra of 139 select OOMs produced from α-pinene ozonolysis will be available at a public data repository site.

Competing Interests

At least one of the (co-)authors is a member of the editorial board of Atmospheric Chemistry and Physics. The authors declare no other competing interests.

https://doi.org/10.5194/egusphere-2024-2454
Preprint. Discussion started: 6 August 2024

References:

Atkinson, R., D. L. Baulch, R. A. Cox, J. N. Crowley, R. F. Hampson, R. G. Hynes, M. E. Jenkin, M. J. Rossi, J. Troe, and I. Subcommittee (2006), Evaluated kinetic and photochemical data for atmospheric chemistry: Volume II – gas phase reactions of organic species, *Atmos. Chem. Phys.*, *6*(11), 3625-4055, doi:10.5194/acp-6-3625-2006.

Aumont, B., S. Szopa, and S. Madronich (2005), Modelling the evolution of organic carbon during its gas-phase tropospheric oxidation: development of an explicit model based on a self generating approach, *Atmos. Chem. Phys.*, *15*, 2497-2517, doi:Doi: 10.5194/acp-5-2497-2005.

Barsanti, K. C., J. H. Kroll, and J. A. Thornton (2017), Formation of Low-Volatility Organic Compounds in the Atmosphere: Recent Advancements and Insights, *The Journal of Physical Chemistry Letters*, *8*(7), 1503-1511, doi:10.1021/acs.jpclett.6b02969.

Bianchi, F., et al. (2019), Highly Oxygenated Organic Molecules (HOM) from Gas-Phase Autoxidation Involving Peroxy Radicals: A Key Contributor to Atmospheric Aerosol, *Chemical Reviews*, *119*(6), 3472-3509, doi:10.1021/acs.chemrev.8b00395.

Camredon, M., B. Aumont, J. Lee-Taylor, and S. Madronich (2007), The SOA/VOC/NO_x system: an explicit model of secondary organic aerosol formation, *Atmos. Chem. Phys.*, *7*(21), 5599-5610, doi:10.5194/acp-7-5599-2007.

Caudillo, L., et al. (2021), Chemical composition of nanoparticles from α-pinene nucleation and the influence of isoprene and relative humidity at low temperature, *Atmos. Chem. Phys.*, *21*(22), 17099-17114, doi:10.5194/acp-21-17099-2021.

Claflin, M. S., J. E. Krechmer, W. Hu, J. L. Jimenez, and P. J. Ziemann (2018), Functional Group Composition of Secondary Organic Aerosol Formed from Ozonolysis of α-Pinene Under High VOC and Autoxidation Conditions, *ACS Earth and Space Chemistry*, *2*(11), 1196-1210, doi:10.1021/acsearthspacechem.8b00117.

Donahue, N. M., S. A. Epstein, S. N. Pandis, and A. L. Robinson (2011), A two-dimensional volatility basis set: 1. organic-aerosol mixing thermodynamics, *Atmos. Chem. Phys.*, *11*(7), 3303-3318, doi:10.5194/acp-11-3303-2011.

Du, M., A. Voliotis, Y. Shao, Y. Wang, T. J. Bannan, K. L. Pereira, J. F. Hamilton, C. J. Percival, M. R. Alfarra, and G. McFiggans (2022), Combined application of online FIGAERO-CIMS and offline LC-Orbitrap mass spectrometry (MS) to characterize the chemical composition of secondary organic aerosol (SOA) in smog chamber studies, *Atmos. Meas. Tech.*, *15*(14), 4385-4406, doi:10.5194/amt-15-4385-2022.

Glasius, M., M. Lahaniati, A. Calogirou, D. Di Bella, N. R. Jensen, J. Hjorth, D. Kotzias, and B. R. Larsen (2000), Carboxylic Acids in Secondary Aerosols from Oxidation of Cyclic Monoterpenes by Ozone, *Environmental Science & Technology*, *34*(6), 1001-1010, doi:10.1021/es990445r.

Hallquist, M., et al. (2009), The formation, properties and impact of secondary organic aerosol: current and emerging issues, *Atmos. Chem. Phys.*, *9*(14), 5155-5236, doi:10.5194/acp-9-5155-2009.

Heinritzi, M., et al. (2020), Molecular understanding of the suppression of new-particle formation by isoprene, *Atmos. Chem. Phys.*, *20*(20), 11809-11821, doi:10.5194/acp-20-11809-2020.

Huang, Y., C. M. Kenseth, N. F. Dalleska, and J. H. Seinfeld (2020), Coupling Filter-Based Thermal Desorption Chemical Ionization Mass Spectrometry with Liquid Chromatography/Electrospray Ionization Mass Spectrometry for Molecular Analysis of Secondary Organic Aerosol, *Environmental Science & Technology*, *54*(20), 13238-13248, doi:10.1021/acs.est.0c01779.

Hyttinen, N., M. Wolf, M. P. Rissanen, M. Ehn, O. Peräkylä, T. Kurtén, and N. L. Prisle (2021), Gas-to-Particle Partitioning of Cyclohexene- and α-Pinene-Derived Highly Oxygenated

https://doi.org/10.5194/egusphere-2024-2454
Preprint. Discussion started: 6 August 2024

Dimers Evaluated Using COSMOtherm, *The Journal of Physical Chemistry A*, *125*(17), 3726-3738, doi:10.1021/acs.jpca.0c11328.

Jenkin, M. E., R. Valorso, B. Aumont, M. J. Newland, and A. R. Rickard (2020), Estimation of rate coefficients for the reactions of O3 with unsaturated organic compounds for use in automated mechanism construction, *Atmos. Chem. Phys.*, *20*(21), 12921-12937, doi:10.5194/acp-20-12921-2020.

Jenkin, M. E., R. Valorso, B. Aumont, and A. R. Rickard (2019), Estimation of rate coefficients and branching ratios for reactions of organic peroxy radicals for use in automated mechanism construction, *Atmos. Chem. Phys.*, *19*(11), 7691-7717, doi:10.5194/acp-19-7691-2019.

Jenkin, M. E., R. Valorso, B. Aumont, A. R. Rickard, and T. J. Wallington (2018), Estimation of rate coefficients and branching ratios for gas-phase reactions of OH with aliphatic organic compounds for use in automated mechanism construction, *Atmos. Chem. Phys.*, *18*(13), 9297-9328, doi:10.5194/acp-18-9297-2018.

Jenkin, M. E., J. C. Young, and A. R. Rickard (2015), The MCM v3.3.1 degradation scheme for isoprene, *Atmos. Chem. Phys.*, *15*(20), 11433-11459, doi:10.5194/acp-15-11433-2015.

Kahnt, A., R. Vermeylen, Y. Iinuma, M. Safi Shalamzari, W. Maenhaut, and M. Claeys (2018), High-molecular-weight esters in α-pinene ozonolysis secondary organic aerosol: structural characterization and mechanistic proposal for their formation from highly oxygenated molecules, *Atmos. Chem. Phys.*, *18*(11), 8453-8467, doi:10.5194/acp-18-8453-2018.

Kenseth, C. M., N. J. Hafeman, S. P. Rezgui, J. Chen, Y. Huang, N. F. Dalleska, H. G. Kjaergaard, B. M. Stoltz, J. H. Seinfeld, and P. O. Wennberg (2023), Particle-phase accretion forms dimer esters in pinene secondary organic aerosol, *Science*, *382*(6672), 787-792, doi:doi:10.1126/science.adi0857.

Kenseth, C. M., Y. Huang, R. Zhao, N. F. Dalleska, J. C. Hethcox, B. M. Stoltz, and J. H. Seinfeld (2018), Synergistic O₃ + OH oxidation pathway to extremely low-volatility dimers revealed in β-pinene secondary organic aerosol, *Proceedings of the National Academy of Sciences*, *115*(33), 8301-8306, doi:doi:10.1073/pnas.1804671115.

Kristensen, K., Å. K. Watne, J. Hammes, A. Lutz, T. Petäjä, M. Hallquist, M. Bilde, and M. Glasius (2016), High-Molecular Weight Dimer Esters Are Major Products in Aerosols from α-Pinene Ozonolysis and the Boreal Forest, *Environmental Science & Technology Letters*, *3*(8), 280-285, doi:10.1021/acs.estlett.6b00152.

Kurtén, T., K. Tiusanen, P. Roldin, M. Rissanen, J.-N. Luy, M. Boy, M. Ehn, and N. Donahue (2016), α-Pinene Autoxidation Products May Not Have Extremely Low Saturation Vapor Pressures Despite High O:C Ratios, *The Journal of Physical Chemistry A*, *120*(16), 2569-2582, doi:10.1021/acs.jpca.6b02196.

Lee, B. H., F. D. Lopez-Hilfiker, C. Mohr, T. Kurtén, D. R. Worsnop, and J. A. Thornton (2014), An Iodide-Adduct High-Resolution Time-of-Flight Chemical-Ionization Mass Spectrometer: Application to Atmospheric Inorganic and Organic Compounds, *Environmental Science & Technology*, *48*(11), 6309-6317, doi:10.1021/es500362a.

Lee, S.-H., H. Gordon, H. Yu, K. Lehtipalo, R. Haley, Y. Li, and R. Zhang (2019), New Particle Formation in the Atmosphere: From Molecular Clusters to Global Climate, *Journal of Geophysical Research: Atmospheres*, *124*(13), 7098-7146, doi:10.1029/2018JD029356.

Lopez-Hilfiker, F. D., et al. (2015), Phase partitioning and volatility of secondary organic aerosol components formed from α-pinene ozonolysis and OH oxidation: the importance of accretion products and other low volatility compounds, *Atmos. Chem. Phys.*, *15*(14), 7765-7776, doi:10.5194/acp-15-7765-2015.

Lopez-Hilfiker, F. D., et al. (2014), A novel method for online analysis of gas and particle composition: description and evaluation of a Filter Inlet for Gases and AEROsols (FIGAERO), *Atmos. Meas. Tech.*, *7*, 983-1001, doi:Doi: 10.5194/amt-7-983-2014.

https://doi.org/10.5194/egusphere-2024-2454
Preprint. Discussion started: 6 August 2024

McFiggans, G., et al. (2019), Secondary organic aerosol reduced by mixture of atmospheric vapours, *Nature*, *565*(7741), 587-593, doi:10.1038/s41586-018-0871-y.

Mehra, A., et al. (2020), Evaluation of the chemical composition of gas- and particle-phase products of aromatic oxidation, *Atmos. Chem. Phys.*, *20*(16), 9783-9803, doi:10.5194/acp-20-9783-2020.

Müller, L., M. C. Reinnig, J. Warnke, and T. Hoffmann (2008), Unambiguous identification of esters as oligomers in secondary organic aerosol formed from cyclohexene and cyclohexene/α-pinene ozonolysis, *Atmos. Chem. Phys.*, *8*(5), 1423-1433, doi:10.5194/acp-8-1423-2008.

Nozière, B., et al. (2015), The Molecular Identification of Organic Compounds in the Atmosphere: State of the Art and Challenges, *Chemical Reviews*, *115*(10), 3919-3983, doi:10.1021/cr5003485.

Pankow, J. F., and W. E. Asher (2008), SIMPOL.1: a simple group contribution method for predicting vapor pressures and enthalpies of vaporization of multifunctional organic compounds, *Atmos. Chem. Phys.*, *8*(10), 2773-2796, doi:10.5194/acp-8-2773-2008.

Peräkylä, O., et al. (2023), Large Gas-Phase Source of Esters and Other Accretion Products in the Atmosphere, *Journal of the American Chemical Society*, *145*(14), 7780-7790, doi:10.1021/jacs.2c10398.

Pospisilova, V., et al. (2020), On the fate of oxygenated organic molecules in atmospheric aerosol particles, *Science Advances*, *6*(11), eaax8922, doi:doi:10.1126/sciadv.aax8922.

Resch, J., K. Wolfer, A. Barth, and M. Kalberer (2023), Effects of storage conditions on the molecular-level composition of organic aerosol particles, *Atmos. Chem. Phys.*, *23*(16), 9161-9171, doi:10.5194/acp-23-9161-2023.

Shao, Y., A. Voliotis, M. Du, Y. Wang, K. Pereira, J. Hamilton, M. R. Alfarra, and G. McFiggans (2022), Chemical composition of secondary organic aerosol particles formed from mixtures of anthropogenic and biogenic precursors, *Atmos. Chem. Phys.*, *22*(15), 9799-9826, doi:10.5194/acp-22-9799-2022.

Tiszenkel, L., and S.-H. Lee (2023), Synergetic Effects of Isoprene and HOx on Biogenic New Particle Formation, *Geophysical Research Letters*, *50*(14), e2023GL103545, doi:https://doi.org/10.1029/2023GL103545.

Tiszenkel, L., C. Stangl, J. Krasnomowitz, Q. Ouyang, H. Yu, M. J. Apsokardu, M. V. Johnston, and S. H. Lee (2019), Temperature effects on sulfuric acid aerosol nucleation and growth: initial results from the TANGENT study, *Atmos. Chem. Phys.*, *19*(13), 8915-8929, doi:10.5194/acp-19-8915-2019.

Tolocka, M. P., M. Jang, J. M. Ginter, F. J. Cox, R. M. Kamens, and M. V. Johnston (2004), Formation of Oligomers in Secondary Organic Aerosol, *Environmental Science & Technology*, *38*(5), 1428-1434, doi:10.1021/es035030r.

Tomaz, S., et al. (2021), Structures and reactivity of peroxy radicals and dimeric products revealed by online tandem mass spectrometry, *Nature Communications*, *12*(1), 300, doi:10.1038/s41467-020-20532-2.

Valorso, R., B. Aumont, M. Camredon, T. Raventos-Duran, C. Mouchel-Vallon, N. L. Ng, J. H. Seinfeld, J. Lee-Taylor, and S. Madronich (2011), Explicit modelling of SOA formation from α-pinene photooxidation: sensitivity to vapour pressure estimation, *Atmos. Chem. Phys.*, *11*(14), 6895-6910, doi:10.5194/acp-11-6895-2011.

Wang, S., Y. Zhao, A. W. H. Chan, M. Yao, Z. Chen, and J. P. D. Abbatt (2023), Organic Peroxides in Aerosol: Key Reactive Intermediates for Multiphase Processes in the Atmosphere, *Chemical Reviews*, *123*(4), 1635-1679, doi:10.1021/acs.chemrev.2c00430.

West, C. P., D. Mesa Sanchez, A. C. Morales, Y.-J. Hsu, J. Ryan, A. Darmody, L. V. Slipchenko, J. Laskin, and A. Laskin (2023), Molecular and Structural Characterization of Isomeric Compounds in Atmospheric Organic Aerosol Using Ion Mobility-Mass Spectrometry, *The Journal of Physical Chemistry A*, *127*(7), 1656-1674, doi:10.1021/acs.jpca.2c06459.

https://doi.org/10.5194/egusphere-2024-2454
Preprint. Discussion started: 6 August 2024

Witkowski, B., and T. Gierczak (2014), Early stage composition of SOA produced by α-pinene/ozone reaction: α-Acyloxyhydroperoxy aldehydes and acidic dimers, *Atmospheric Environment*, *95*, 59-70, doi:https://doi.org/10.1016/j.atmosenv.2014.06.018.

Yasmeen, F., R. Vermeylen, R. Szmigielski, Y. Iinuma, O. Böge, H. Herrmann, W. Maenhaut, and M. Claeys (2010), Terpenylic acid and related compounds: precursors for dimers in secondary organic aerosol from the ozonolysis of α- and β-pinene, *Atmos. Chem. Phys.*, *10*(19), 9383-9392, doi:10.5194/acp-10-9383-2010.

Ye, Q., et al. (2019), Molecular Composition and Volatility of Nucleated Particles from α-Pinene Oxidation between −50 °C and +25 °C, *Environmental Science & Technology*, *53*(21), 12357-12365, doi:10.1021/acs.est.9b03265.

Zhang, X., R. C. McVay, D. D. Huang, N. F. Dalleska, B. Aumont, R. C. Flagan, and J. H. Seinfeld (2015), Formation and evolution of molecular products in α-pinene secondary organic aerosol, *Proceedings of the National Academy of Sciences*, *112*(46), 14168-14173, doi:doi:10.1073/pnas.1517742112.

Zhao, R., C. M. Kenseth, Y. Huang, N. F. Dalleska, X. M. Kuang, J. Chen, S. E. Paulson, and J. H. Seinfeld (2018a), Rapid Aqueous-Phase Hydrolysis of Ester Hydroperoxides Arising from Criegee Intermediates and Organic Acids, *The Journal of Physical Chemistry A*, *122*(23), 5190-5201, doi:10.1021/acs.jpca.8b02195.

Zhao, Y., J. A. Thornton, and H. O. T. Pye (2018b), Quantitative constraints on autoxidation and dimer formation from direct probing of monoterpene-derived peroxy radical chemistry, *Proceedings of the National Academy of Sciences*, *115*(48), 12142-12147, doi:10.1073/pnas.1812147115.

Zhao, Y., L. M. Wingen, V. Perraud, J. Greaves, and B. J. Finlayson-Pitts (2015), Role of the reaction of stabilized Criegee intermediates with peroxy radicals in particle formation and growth in air, *Physical Chemistry Chemical Physics*, *17*(19), 12500-12514, doi:10.1039/C5CP01171J.

Zhao, Y., M. Yao, Y. Wang, Z. Li, S. Wang, C. Li, and H. Xiao (2022), Acylperoxy Radicals as Key Intermediates in the Formation of Dimeric Compounds in α-Pinene Secondary Organic Aerosol, *Environmental Science & Technology*, *56*(20), 14249-14261, doi:10.1021/acs.est.2c02090.

Ziemann, P. J., and R. Atkinson (2012), Kinetics, products, and mechanisms of secondary organic aerosol formation, *Chemical Society Reviews*, *41*(19), 6582-6605, doi:10.1039/C2CS35122F.

https://doi.org/10.5194/egusphere-2024-2454
Preprint. Discussion started: 6 August 2024

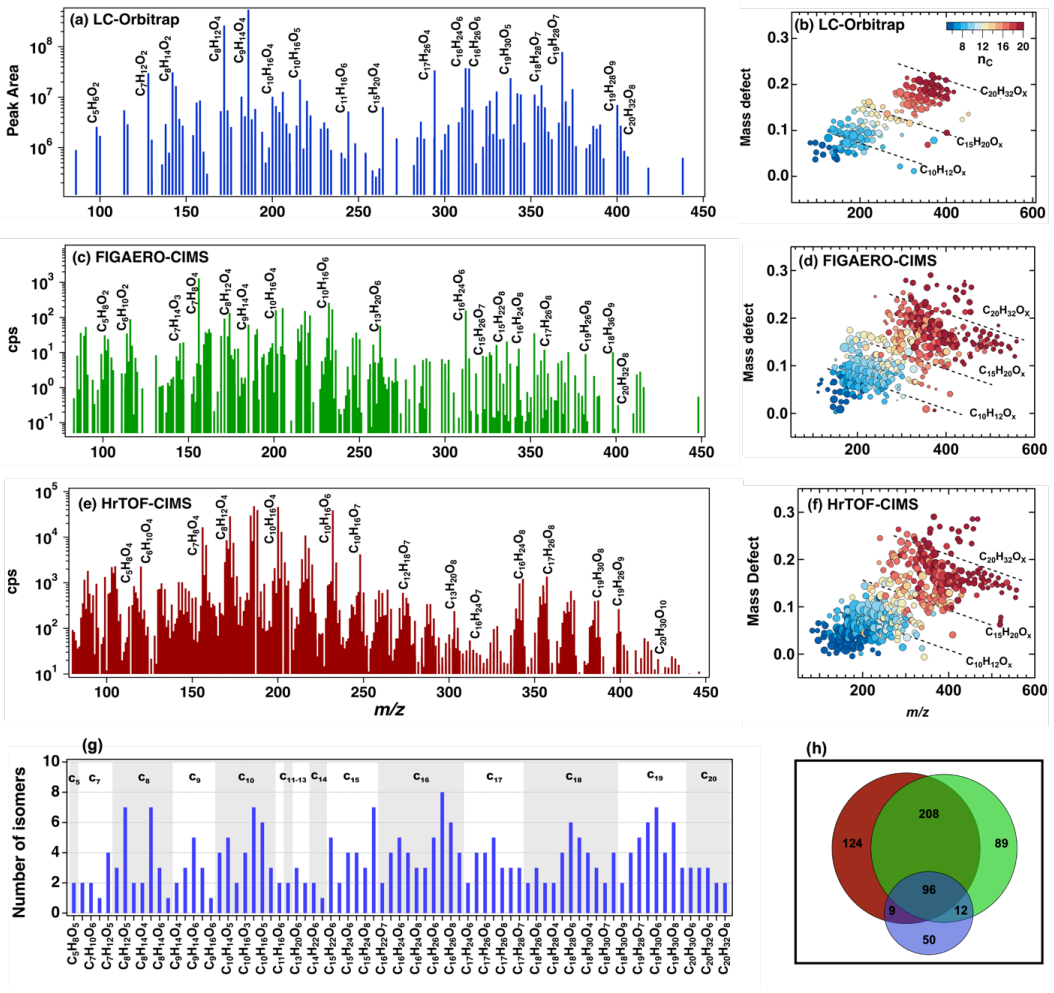

Figure 1. Mass spectra and mass defects of OOMs detected from α-pinene ozonolysis flow-tube experiment, with α-pinene of 238 ppb, ozone of 1.2 ppm, a temperature of 298 K, RH < 10 %, [OH] = 1.6 ppt and residence time = 150 s, in the particles phase using offline UPLC/(-)ESI-Orbitrap MS (a, b) and the particle (c, d) and gas phase (e, f) using FIGAERO-CIMS. (g) The number of isomers identified for each detected OOMs in the particle phase. For clarity, only every other OOMs are shown with their chemical formulas here (see Figure 2c for the entire formulas for all OOMs.) (h) Venn diagram showing the number of compounds detected from the gas phase (red) and particle phase (green) with FIGAERO-CIMS, and in the particle phase with UPLC/(-)ESI-Orbitrap MS (blue).

https://doi.org/10.5194/egusphere-2024-2454
Preprint. Discussion started: 6 August 2024

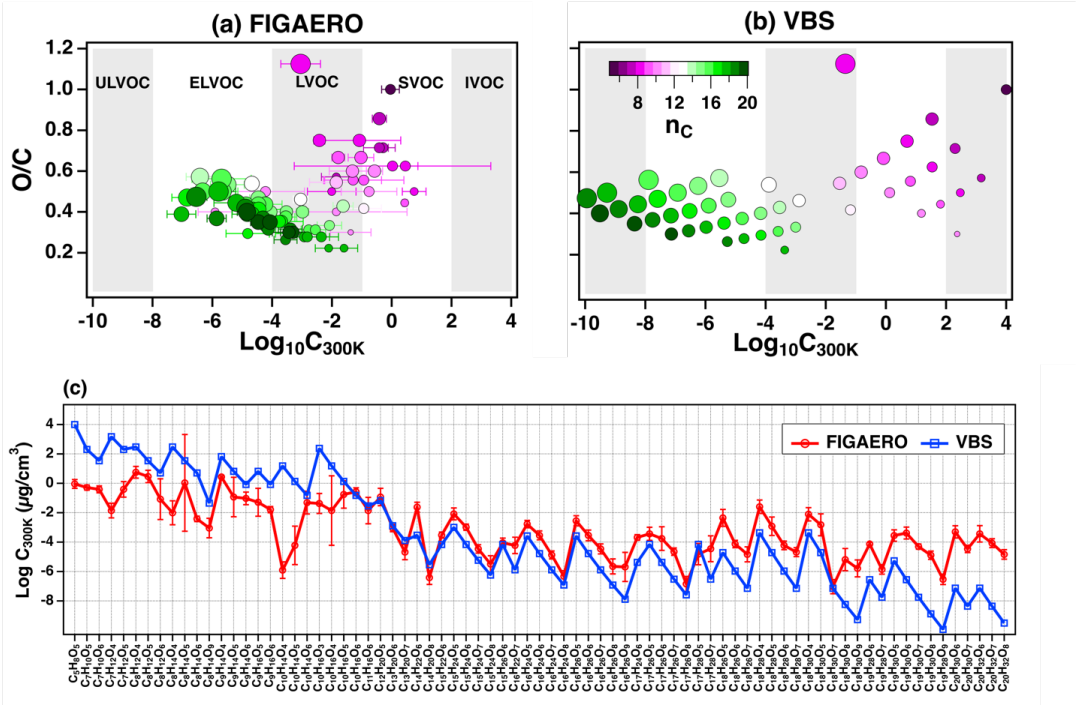

Figure 2. Comparison of saturation vapor concentrations of biogenic OOMs produced from α-pinene ozonolysis indicated by O:C ratio measured with the FIGAERO thermogram (a) and estimated from VBS (b). The color scale represents the number of carbons in the compound and bubble size represents the oxygen numbers. The O/C vs. $Log_{10}C_{300k}$ space is classified into different bins as ultra-low volatility organic compounds (ULVOC); extremely-low volatility organic compounds (ELVOC); low-volatility organic compounds (LVOC); semi-volatile organic compounds (SVOC); and intermediate volatile organic compounds (IVOC). (c) Comparison of the volatilities obtained from the VBS and FIGAERO for each chemical formula of OOMs.

https://doi.org/10.5194/egusphere-2024-2454
Preprint. Discussion started: 6 August 2024

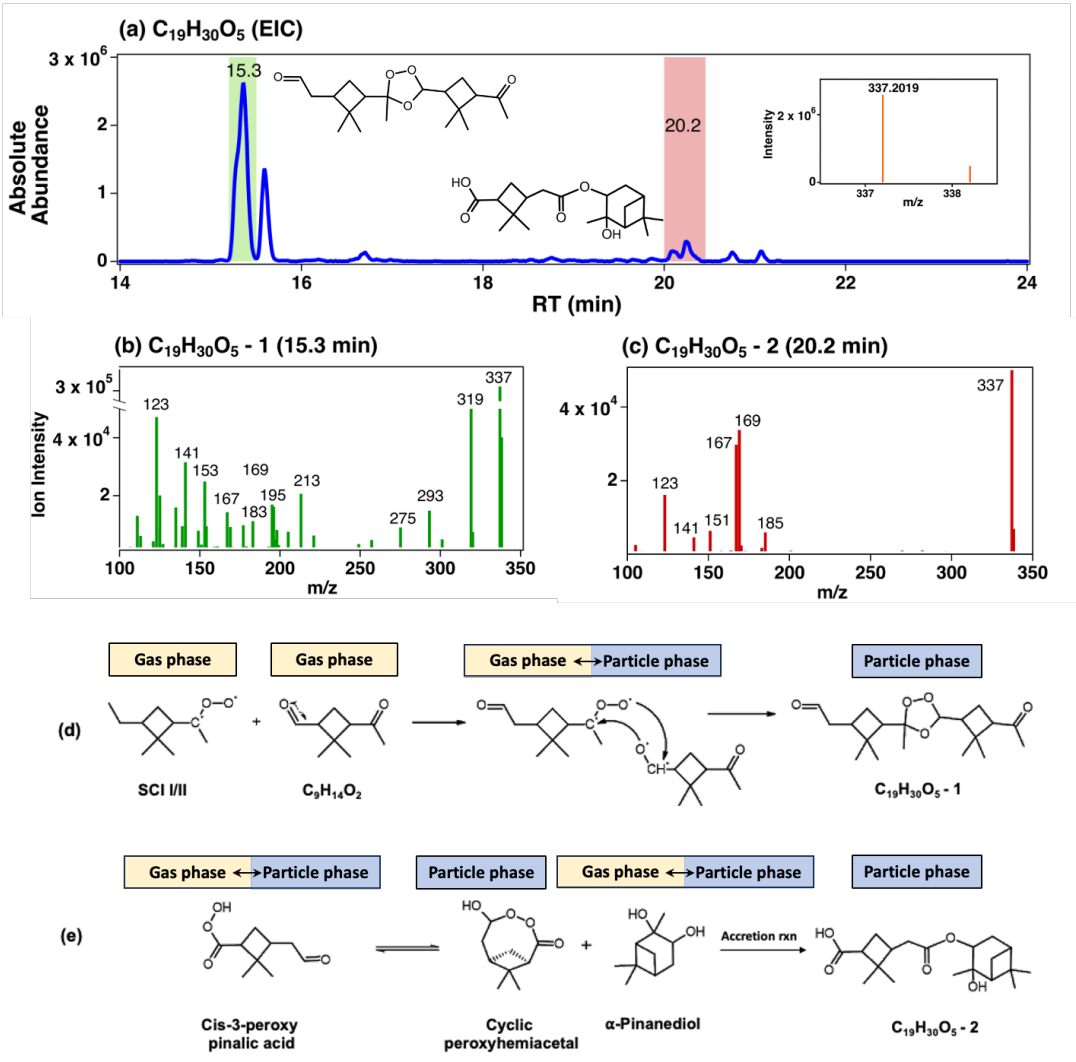

Figure 3. (a) EIC of $C_{19}H_{30}O_5$ (*m/z* = 337.2019). The inset figure shows the MS spectra showing the mass peak of the $C_{19}H_{30}O_5$ at the retention time (RT) of 15.3 min. MS/MS spectra of the isomers with the RT of 15.3 min (b) and 20.2 min (c). Reactions leading to the formation of two isomers, $C_{19}H_{30}O_5$ -1 (d) and (e) $C_{19}H_{30}O_5$ -2 (e). Reactions shown in Figure 3d were proposed in this study. Reactions shown in Figure 3e were adopted from [*Kenseth et al.*, 2023].

https://doi.org/10.5194/egusphere-2024-2454
Preprint. Discussion started: 6 August 2024

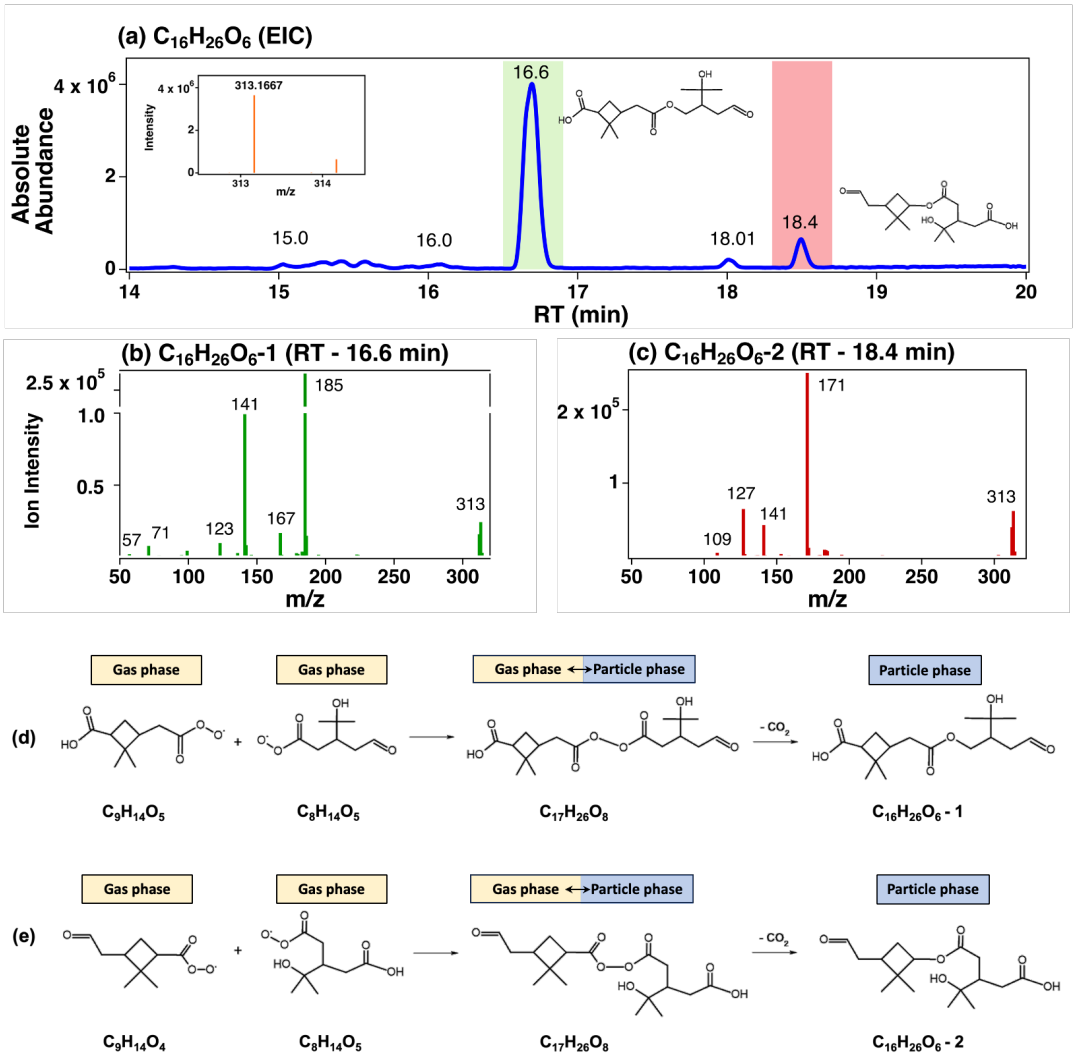

Figure 4. **(a)** EIC of $C_{16}H_{26}O_6$ with its five isomers labeled. The inset figure is the MS spectra showing the mass peak of $C_{16}H_{26}O_6$ at RT = 16.6 min. MS/MS spectrum of two isomers with RT = 16.6 min (b) and RT = 18.4 min (c). Reactions leading to the formation of two isomers, $C_{16}H_{26}O_6$-1 (d) and $C_{16}H_{26}O_6$-2 (e), both proposed in this study.